Amplitude behaviour of geodesic acoustic modes in the ASDEX Upgrade tokamak

G D Conway and the ASDEX Upgrade Team

Max-Planck-Institut für Plasmaphysik, EURATOM-Association IPP, D-85748 Garching, Germany

Abstract. The amplitude behaviour of the geodesic acoustic mode (GAM), a low frequency ($5 - 25$ kHz) coherent plasma turbulence-generated $E_\mathrm{r} \times B$ zonal flow oscillation, is studied in the ASDEX Upgrade tokamak using Doppler reflectometry. Across the tokamak edge the GAM displays one or more maxima a few cm wide, coinciding with radial plateaus in the GAM frequency, suggesting nested zonal flow layers. The GAM peak amplitude ranges between $0.2 - 0.8$ km s^{-1}, corresponding to several tens of percent of the mean $E \times B$ flow velocity. In limiter configurations the GAM amplitude is found to decrease inversely with the plasma vertical elongation $1.1 < \kappa < 1.4$, but rises again in X-point divertor configurations at higher $\kappa \sim 1.6$. At low κ the GAM amplitude increases with the safety factor q, consistent with damping effects, but becomes less sensitive to q at high κ. A positive linear dependence on the electron temperature gradient, an indicator of the linear turbulence drive, is also observed.

PACS numbers: 52.55.Fa, 52.35.Ra, 52.70.Gw

Submitted to: *Plasma Phys. Control. Fusion*

1. Introduction

Geodesic acoustic modes (GAMs) are a form of oscillating zonal flows which appear in a variety of fluid and plasma situations, cf. review by Diamond and references therein [1]. In magnetic confinement devices GAMs appear as low frequency (a few kHz) coherent perturbations in the $E_\mathrm{r} \times B$ poloidal plasma flow with an axisymmetric ($m = n = 0$) mode structure and a finite radial extent ($k_\mathrm{r} a \gg 1$). The flow perturbation couples, via the geodesic curvature of the magnetic field, to an axisymmetric pressure sideband mode ($m = \pm 1, n = 0$) to create an eigenmode oscillation, which is essentially electrostatic (i.e. no strong magnetic component) and is observed only on closed flux surfaces [2].

GAMs, and zonal flows in general, are driven by the plasma turbulence (via non-linear interactions, e.g. Reynolds stress etc.) [3]. In-turn they are believed to moderate the turbulence (and hence anomalous plasma transport) either via radial shearing of turbulence eddies - which reduces the turbulence radial correlation length (shear de-correlation) or by acting as an energy sink [4, 5, 1]. Although the turbulence tends to force the GAM over a broad range of frequencies (the geodesic transfer effect [6, 7]), it has a natural eigenfrequency, which scales as $\omega_\mathrm{GAM} = 2\pi f_\mathrm{GAM} = G\, c_\mathrm{s}/R_\mathrm{o}$, where $c_\mathrm{s} = \sqrt{(T_\mathrm{e} + T_\mathrm{i})/M_\mathrm{i}}$ is the ion sound speed and R_o is the plasma major radius. For circular, large aspect ratio $R_\mathrm{o} \gg a$ plasmas [8] the scale factor is $G \approx \sqrt{2}$. However, for non-circular plasmas experimental measurements show substantial deviations from this simple prediction, with dependences on the plasma vertical elongation κ and the safety factor q, cf. [2, 9, 10, 11]. The amplitude of the GAM oscillation also displays parameter dependencies, particularly on the safety factor [9, 12, 13, 14] which is predicted to control the mode damping, either through collisionless Landau-like damping [15, 16, 17, 18] or via collisional/viscous damping [19].

In addition to damping effects the strength of the turbulence drive and the Reynolds stress coupling should affect the steady-state GAM amplitude. Needless to say, it is important to understand the behaviour of both the GAM amplitude and frequency since the GAM may impact on the $E_\mathrm{r} \times B$ shearing rate and hence turbulence moderation, if, (1) its frequency is lower than the inverse turbulence de-correlation time $f_\mathrm{GAM} < 1/\tau_d$ [4, 5, 20, 16, 21] - which is generally the case in the plasma edge, and (2) its amplitude A_GAM is sufficiently large, e.g. a displacement comparable to the turbulence structure size.

The parameter dependence of the GAM frequency in ohmic and L-mode discharges in the ASDEX Upgrade tokamak have been reported elsewhere [11], here, observations are presented of the GAM amplitude dependence on both plasma configuration parameters (damping) and profile gradients (driving) using Doppler microwave reflectometry to directly measure perturbations in the $E \times B$ flow velocity. By keeping other parameters constant a series of scans in temperature gradient (showing a linear increase of A_GAM), elongation (reciprocal decrease) and q (complex behaviour) are obtained. The radial position of the GAM maxima is also seen to vary with the plasma parameters.

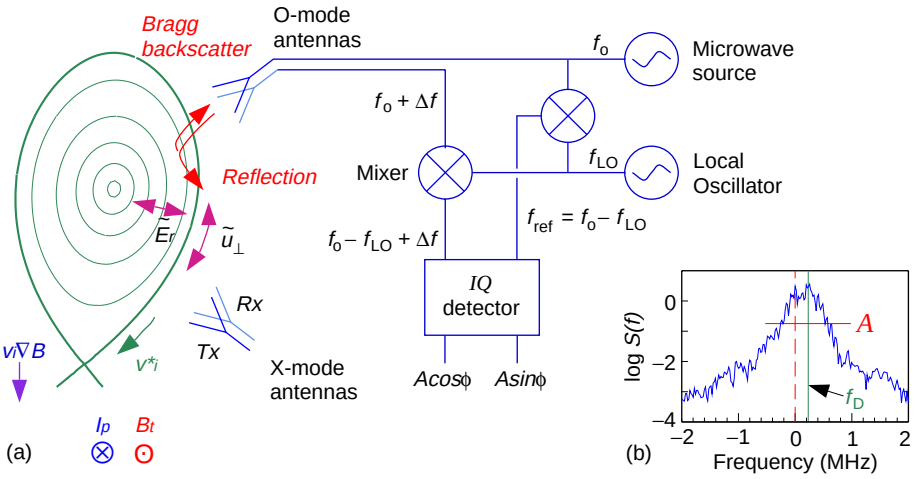

Figure 1. (a) Schematic of Doppler reflectometer diagnostic and poloidal location of O and X-mode antenna pairs in AUG tokamak, and (b) typical complex amplitude reflectometer spectrum from an ohmic discharge.

2. Measurement technique

On the ASDEX Upgrade tokamak (AUG) microwave Doppler reflectometry has been used extensively to measure the $E_r \times B$ plasma flow velocity and its fluctuations [2, 10, 11, 12, 22, 23, 24]. The diagnostic technique is shown schematically in figure 1. A microwave beam is launched into the plasma at an angle θ_o to the flux surface where it experiences refraction, and eventually reflection at the cutoff condition when the refractive index squared approaches a minimum: $N^2 = \sin^2\theta_o$ for a flat cutoff layer. The presence of moving turbulence in the cutoff region causes backscattering of the beam - providing there is sufficient turbulence containing a perpendicular wavenumber satisfying the Bragg condition, $k_\perp = 2k_o N$, where k_o is the probing wavenumber - which is Doppler frequency shifted by $f_D = u_\perp k_\perp / 2\pi$, where $u_\perp = v_{E\times B} + v_{\text{phase}}$ is the perpendicular (to the static magnetic field) velocity of the turbulence moving in the plasma. Since $u_\perp$ contains the $E_r \times B$ velocity, fluctuations in the radial electric field E_r appear directly as fluctuations in the Doppler frequency.

In the experiment the Doppler frequency is obtained from the complex amplitude spectrum of the digitized reflectometer in-phase ($I = A\cos\phi$) and quadrature ($Q = A\sin\phi$) signals. An example spectrum from an ohmic discharge is shown in figure 1(b). The f_D is computed from the weighted spectral mean and the backscattered signal amplitude $\mathcal{A}$ (a measure of the density fluctuation $\tilde{n}_e$ at the probed $k_\perp$) from the integrated spectrum. By sliding the FFT window ($N_{FFT} = 256$ points) - used to compute the spectrum - through the I & Q signals a time sequence of f_D and $\mathcal{A}$ fluctuations are produced, which are then spectral analysed to obtain the GAM frequency and amplitude, as illustrated in figure 2(c). By stepping the microwave launch frequency ($50 - 75$ GHz) the measurement location, which is obtained using a beam tracing code and spline fitted density profiles, can be scanned from the plasma edge to around the tokamak mid-radius

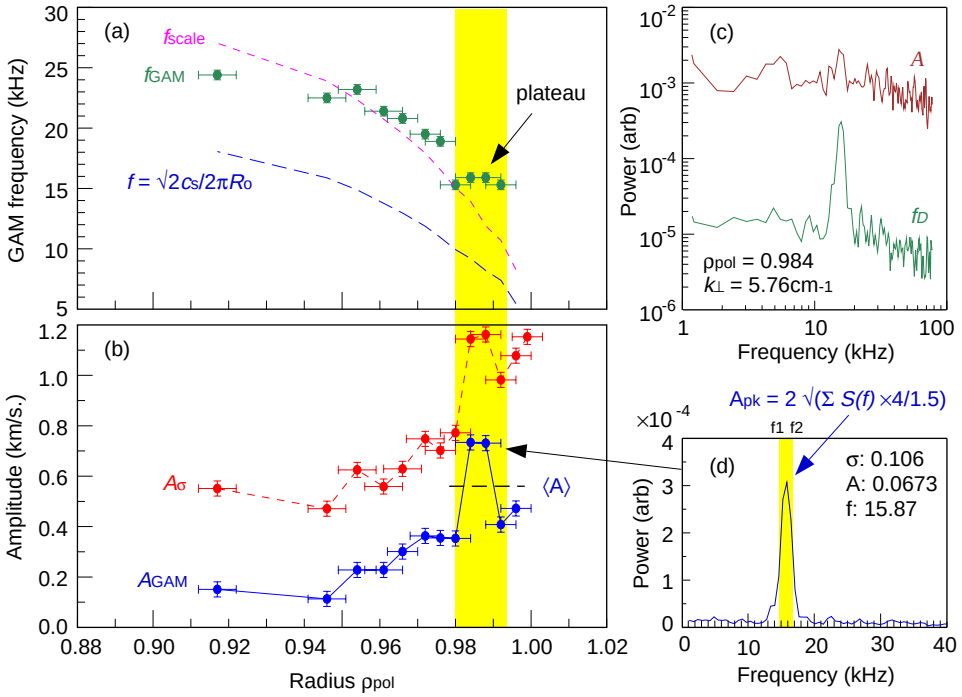

Figure 2. (a) GAM frequency $f_{\rm GAM}$ and (b) GAM peak-to-peak amplitude $A_{\rm GAM}$ and RMS f_D fluctuation A_σ profiles vs radial coordinate $\rho_{\rm pol}$ for circular ohmic limiter shot #20856, with (c & d) $f_{\rm D}$ and $\mathcal{A}$ spectra.

[24]. Full details of the dual O and X-mode polarization, heterodyne reflectometers used are given in [22] and details of the analysis technique in [2].

3. Results

3.1. General GAM features

GAMs are observed in all ohmic and L-mode (neutral beam and electron cyclotron resonance heated) AUG discharges as coherent modes in the $f_{\rm D}$ spectra between $5-25$ kHz with an intensity of 1 to 2 orders of magnitude above the background, with generally only a weak density perturbation, cf. the $\mathcal{A}$ spectrum in figure 2(c). They are normally seen in the edge density gradient region of single-null diverted discharges, but can reach deeper into circular non-diverted limiter discharges [10, 11]. The GAM frequency scales linearly with the ion sound speed over the major radius $f_{\rm GAM} = G\, c_{\rm s}/(2\pi R_{\rm o})$, with no dependence on either the magnetic field B or the mean plasma density $n_{\rm e}$, i.e. the mode is acoustic in nature. Inside the density pedestal radius the scale factor $G \sim \sqrt{2}$ for circular plasmas, as predicted by theory, but in the edge the GAM frequency displays an inverse dependence on the boundary elongation $G \approx 4\pi\{(1+\kappa_{\rm b})^{-1} - \epsilon_o\}$ [11]. Figure 2 shows (a) the GAM frequency $f_{\rm GAM}$ and (b) amplitude $A_{\rm GAM}$ plotted vs the normalized poloidal flux radial coordinate $\rho_{\rm pol}$ for the circular, $\kappa_{\rm b} = 1.09$, limiter ohmic shot #20856. The plot covers about 5 cm of the edge

radius with the radial error bars determined primarily by the beam tracing width and the ambiguity of the density profile fit. The GAM perturbation amplitude is given in terms of a peak-to-peak velocity, which is obtained by integrating over the $S(f_{\rm D})$ spectrum peak [cf. figure 2(d)] and taking the square-root: $A_{\rm [kHz]} = 2\sqrt{(\sum_{f1}^{f2} S(f_{\rm D}) \times 4/1.5)}$. The 4/1.5 factor compensates for the Hanning bell-window, $H_i = \frac{1}{2}\{1 - \cos(2\pi i/N_{\rm FFT})\}$, applied to the signals to minimize spectral leakage. The amplitude (in kHz) is then converted to a velocity by $A_{\rm GAM} = 2\pi\, A_{\rm [kHz]}/k_\perp$. For ohmic and L-mode conditions the mean $u_\perp$ velocity is typically of the order of $2 - 5$ km s^{-1} across the edge region where the GAM peaks (cf. [22]), thus the measured GAM peak amplitudes of $0.2 - 0.8$ km s^{-1} represent perturbations of $10 - 30\%$ of the mean flow - which is not insubstantial. However, in physical terms these amplitudes translate to poloidal displacements of $A_{\rm GAM}/\omega_{\rm GAM} \sim 0.4 - 1$ cm.

3.2. Amplitude radial profiles

Figure 3(a) shows a series of radial profiles of the GAM amplitude (as velocity perturbation) vs $\rho_{\rm pol}$ for a wide range of ohmic and L-mode (ECRH and NBI) discharges with various boundary elongation, $1.09 < \kappa_{\rm b} < 1.74$, and edge safety factors, $3.0 < q_{95} < 4.2$. Each profile displays one or more radial peaks with the most intense generally appearing in the edge density gradient region. However, in all cases, the stronger the peak the further out radially it is located, i.e. towards higher q values. Replotting the radial data against the corresponding local q (obtained from the CLISTE equilibrium code [25] using magnetic data only) in figure 3(b) illustrates more clearly the increasing GAM peak amplitude with q. Indeed, for low κ circular plasmas touching the inner limiter (circular points) the envelope of the GAM maxima (points with error bars) appears almost linear. At low $q \sim 2$ no GAMs are detectable above the background spectrum, and in particular for circular plasmas the radial extent of the GAM is dictated by the q profile, as seen in figure 3(a) where the inner reach increases with q_{95}. However, for plasmas with an X-point divertor configuration at higher κ the density pedestal is much more pronounced, i.e. a large second radial derivative $(\partial^2/\partial r^2)$ in the profile, which now appears to act as a stronger boundary so that no GAMs are seen inside of the pedestal top at $\rho_{\rm pol} \sim 0.94$ [11]. In addition, the GAM peaks tend to be smaller than for equivalent limiter configurations. Overall, there is no clear preferred radial position for the GAM maxima, and there is no alignment with any rational q surface. The radial peaks tend to become broader towards the core as the q profile becomes shallower.

In AUG ohmic and L-mode conditions the majority of the plasma column is in the low collisionality plateau and banana regimes [23]. Here, linear theory predicts that the GAM amplitude should be dominated by collisionless Landau-like damping mechanisms with a damping rate $\gamma \sim \exp(-q^2)$ [15, 16, 18]. In figure 3(c) the GAM amplitude decreases with increasing $\gamma = \omega_{\rm GAM} \exp(-q^2)$ at low q values. But at higher q the amplitude saturates, and then begins to fall. For $q_{95} \to 6$ no GAMs have been observed. At high densities (and q) the edge collisionality in AUG approaches the Pfirsch-Schlüter

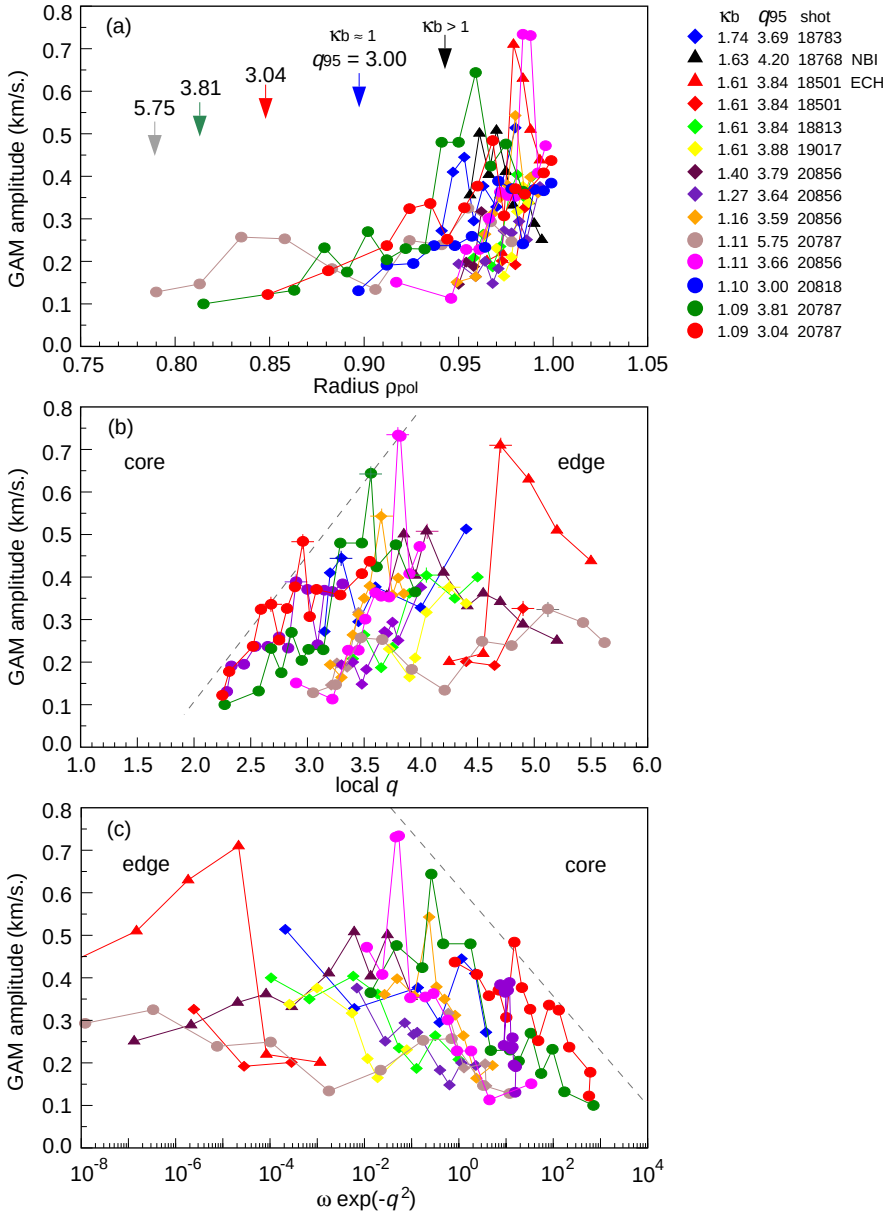

Figure 3. GAM amplitude vs (a) radius ρ_{pol}, (b) local q, and (c) linear growth rate $\gamma = \omega_{\rm GAM}\exp(-q^2)$ for a range of ohmic and L-mode shots with various boundary elongation $\kappa_{\rm b}$ and q_{95}.

limit $\nu^*\epsilon^{3/2} = 1$, where $\nu^* = \nu_{\rm ei}/(\epsilon\omega_{\rm be})$ is the normalized collisionality and $\epsilon = r/R_{\rm o}$ the inverse aspect ratio. Here, the GAM maybe dominated more by collisional damping, for which Novakovskii gives a damping rate $\gamma \approx 4\nu_{ii}/(7q)$ [19] with a weaker q dependence.

The q value, however, is not the only parameter affecting the steady-state GAM amplitude. In addition to the κ reduction seen in figure 3 the effect of increased turbulence drive with additional heating is also evident in stronger L-mode peaks with equivalent κ and q_{95}.

4. Parameter dependence

Figure 2(a) shows the GAM frequency is not a smooth function of radius but has a staircase form with a series of plateaus a few cm wide. The plateaus become progressively wider with decreasing radius and generally coincide with regions of enhanced GAM amplitude A_{GAM}, which suggests a series of nested zonal layers. The mean GAM frequency nevertheless follows a $c_{\mathrm{s}}/R_{\mathrm{o}}$ scaling. Overlayed in figure 2(a) are the predicted GAM frequency for a large aspect ratio circular plasma and a heuristic scaling model with a κ dependence. The edge and core frequency behaviour is discussed in more detail elsewhere [11].

As shown in figure 3(a) the GAM radial peak can be quite narrow in the edge with perhaps just a single measurement point around the maxima. Therefore, to provide a more robust measure of the GAM strength a radial average of the amplitude $\langle A_{\mathrm{GAM}} \rangle$ is taken over the frequency plateau region, as illustrated in figure 2(b). This mean amplitude is now used to investigate the various parameter dependencies, specifically the q, the elongation κ_{b} and the turbulence drive.

The density fluctuation level of gradient driven turbulence, such as ion temperature gradient (ITG) or electron drift wave turbulence scales roughly with the gradient, e.g. $\tilde{n}/n \sim (k_{\perp} L_n)^{-1}$ where $L_n = |n/(dn/dr)|$ is the density gradient scale length (cf. [26]). Many theoreticians also employ a normalized gradient length such as R/L_n, or R/L_T etc. Unfortunately, a meaningful scale length can be difficult to ascribe in the tokamak edge region where its value changes substantially across the GAM plateau radius. Instead a normalized electron temperature gradient $\nabla T_{\mathrm{e}}/\sqrt{\kappa_{\mathrm{b}}}$ is chosen to indicate the turbulence drive, since, in the edge pedestal region of AUG the density and temperature gradients are roughly coupled, such that $\eta_e = L_n/L_{T_{\mathrm{e}}} \approx 2$ [27], and experimentally the electron temperature can be measured with better resolution than the density using ECE diagnostics. The $\sqrt{\kappa}$ normalization is required to convert the gradient to a flux surface constant parameter.

4.1. q dependence

In figure 4(a) the mean amplitude $\langle A_{\mathrm{GAM}} \rangle$ is plotted vs q_{95} for a series of shots with different I_p and B_T but similar normalized electron temperature gradients of $\nabla T_{\mathrm{e}}/\sqrt{\kappa_{\mathrm{b}}} \approx 3.45$ keV m^{-1}. Two groups of boundary elongation are shown: circular limiter $\kappa_{\mathrm{b}} = 1.1$ (blue closed symbols) and elongated divertor $\kappa_{\mathrm{b}} = 1.6$ (red open symbols). In figure 4(b) the data are plotted against the corresponding local q value at the GAM radial maxima with the error bars representing the variation in q across the GAM plateau. For the circular shape the GAM amplitude increases linearly with q, which would be consistent with decreasing damping. However, the elongated divertor shape displays the opposite trend, decreasing slightly with q, or at best remaining approximately constant. Nevertheless, the GAM maximum generally moves radially outward with increasing q_{95}.

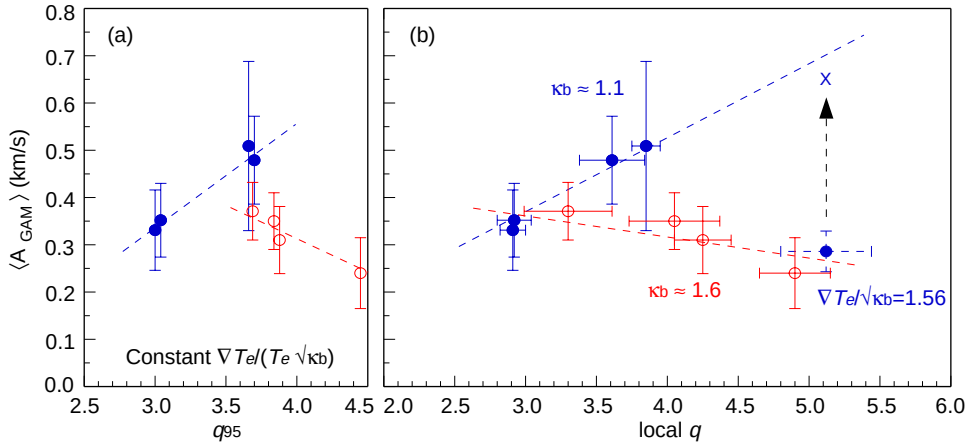

Figure 4. Mean GAM amplitude $\langle A_{\mathrm{GAM}} \rangle$ vs (a) edge q_{95} and (b) local q with fixed normalized temperature gradient $\nabla T_{\mathrm{e}}/\sqrt{\kappa}_{\mathrm{b}} \sim 3.45$ for ohmic shots with boundary elongation $\kappa_{\mathrm{b}} = 1.1$ (blue closed symbols) and $\kappa_{\mathrm{b}} = 1.6$ (red open symbols).

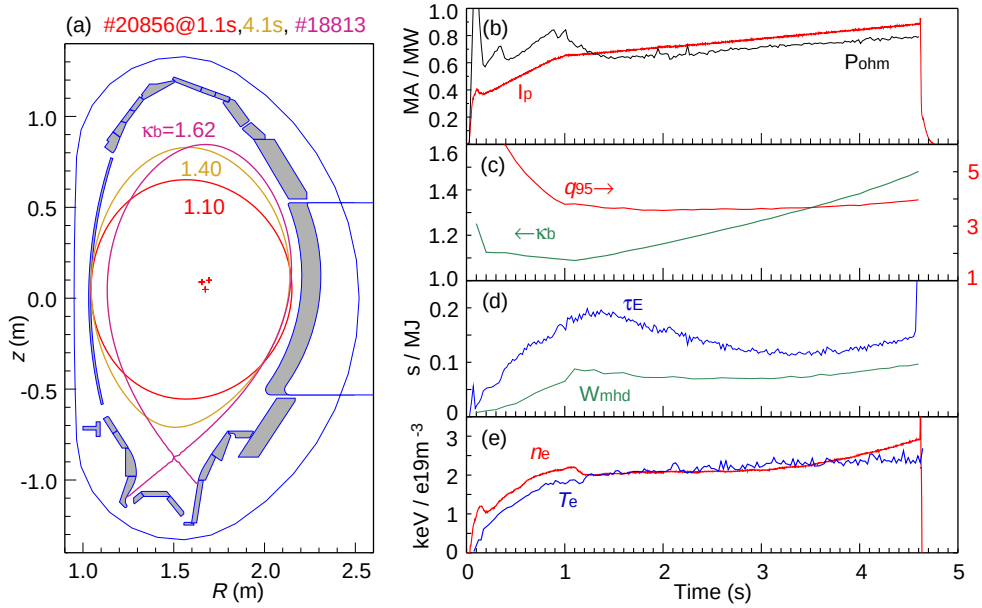

Figure 5. (a) Flux surface boundary contours, plus time traces of (b) plasma current I_{p} and ohmic power P_{ohm}, (c) boundary elongation κ_{b} and q_{95}, (d) global energy confinement time τ_{E} and stored energy W_{mhd} and (e) line average central density and core electron temperature for ohmic limiter shot #20856.

4.2. κ dependence

In ASDEX Upgrade the plasma shape (elongation κ and triangularity δ) is controlled by active external coils and the internal passive structures [28]. The highest elongation obtainable is in a lower single-null divertor configuration, with a boundary elongation between $1.4 < \kappa_{\mathrm{b}} < 1.75$, while in non-diverted configurations the elongation can be reduced down to almost circular, $1.09 < \kappa_{\mathrm{b}} < 1.48$ with the plasma touching the inner limiter - as shown in the flux boundary poloidal contour plots in figure 5(a).

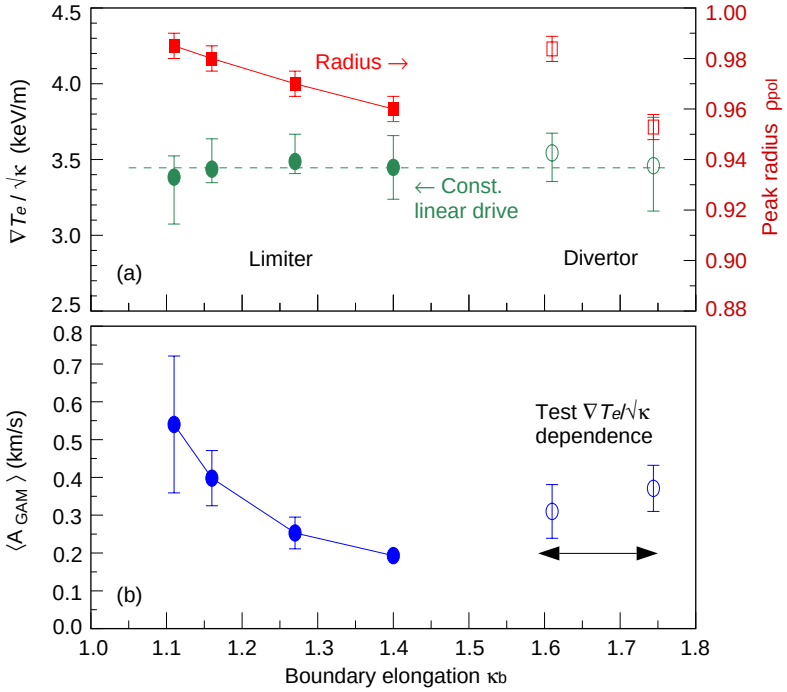

Figure 6. (a) Normalized electron temperature gradient $\nabla T_e/\sqrt{\kappa_b}$ and (b) mean GAM amplitude $\langle A_{GAM}\rangle$ vs boundary elongation κ_b at fixed $q_{95} \approx 3.66$, during I_p ramp in ohmic limiter shot #20856 (solid symbols) and selected divertor shots (open symbols).

Figure 5(b) shows parameter time traces of the $B_T = -1.95$ T ohmic inner limiter shot #20856 where the elongation is ramped up from $\kappa_b = 1.09$ to around 1.4. The plasma volume correspondingly increases by about 20% from 10.53 to 12.74 m^{-3} with elongation, but by ramping the plasma current $I_p = 0.67 \rightarrow 0.85$ MA a roughly constant $q_{95} \approx 3.66$ is maintained. With judicious gas fuelling a steady average density and core temperature are obtained with a constant normalized temperature gradient of $\nabla T_e/\sqrt{\kappa_b} \approx 3.4$ keV m^{-1}. Note that the corresponding normalized temperature scale length $\nabla T_e/(T_e\sqrt{\kappa_b})$ is also constant at any fixed radius.

The resulting mean GAM amplitude $\langle A_{GAM}\rangle$ vs boundary elongation (with constant linear turbulence drive and q_{95}) is shown in figure 6. As the elongation increases the GAM amplitude decreases inversely (solid symbols). The GAM peak position also moves radially inward to a lower q location - consistent with a higher damping - however, the change in the local q from 3.70 to 3.35 is not enough, as shown in figure 4, to account for the drop in $\langle A_{GAM}\rangle$.

The inverse amplitude variation with κ_b suggests an asymptotic, or at least a weak variation at larger values of κ_b. Since the current GAM database is also more extensive at higher κ (together with the consequent weaker q dependence) this appears to be a good place to test for a dependence on the gradient drive. However, larger elongation means moving to the divertor shape. Two representative points from diverted shots at similar q_{95} and ∇T_e are included in figure 6 (open symbols). The amplitudes are

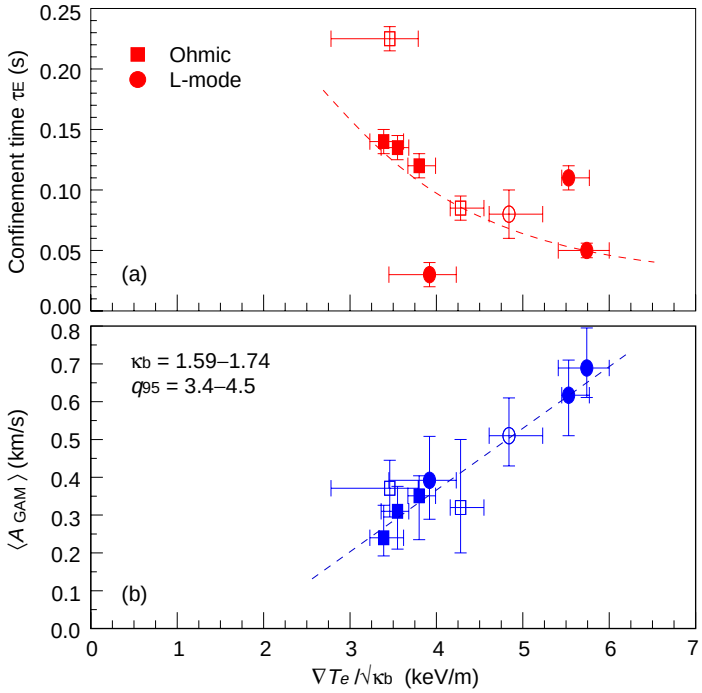

Figure 7. (a) Energy confinement time $\tau_{\rm E}$ and (b) mean GAM amplitude $\langle A_{\rm GAM}\rangle$ vs normalized temperature gradient $\nabla T_{\rm e}/\sqrt{\kappa_{\rm b}}$ for range of ohmic (squares) and L-mode (circles) shots with restricted elongation $\kappa_{\rm b} \sim 1.59 - 1.74$ and $q_{95} \sim 3.4 - 4.5$, $I_{\rm p} = 0.8$ (closed symbols) and 1.0 MA (open symbols).

distinctly larger than the highest $\kappa_{\rm b}$ limiter point, but nevertheless the $\kappa_{\rm b}$ dependence appears to be weak, if somewhat positive.

4.3. $\nabla T_{\rm e}$ dependence

Figure 7 shows (a) the global energy confinement time $\tau_{\rm E}$ and (b) the mean GAM amplitude $\langle A_{\rm GAM}\rangle$ as a function of the normalized temperature gradient $\nabla T_{\rm e}/\sqrt{\kappa_{\rm b}}$ for range of ohmic (squares) and L-mode (circles) shots with plasma current $I_{\rm p} = 0.8$ MA (closed symbols) and 1.0 MA (open symbols) and a restricted $\kappa_{\rm b} = 1.64 \pm 0.05$ and $q_{95} \sim 3.9 \pm 0.4$ divertor X-point configuration. The GAM amplitude increases linearly with the gradient and is accompanied by a corresponding decrease in the global confinement, due, one expects, to increasing turbulence transport. The GAM amplitude appears to increase right upto the L to H-mode threshold. The disappearance of the GAM in the H-mode, despite the generally higher edge gradients, reflects the bifurcation nature of the transition.

The linear scaling of the GAM amplitude with the gradient has a non-zero intersect, which implies a threshold in the temperature/density gradient for the GAM onset. However, such a threshold may not be constant. The limited data available at lower $\kappa_{\rm b}$ indicates that the curve would move to the left, to lower $\nabla T_{\rm e}$ values with decreasing elongation. In figure 4(b) an additional $\kappa_{\rm b} = 1.1$ point at high q is included, but with a lower $\nabla T_{\rm e}/\sqrt{\kappa_{\rm b}} = 1.56$ keV m^{-1} (dashed error bars). However, if the GAM amplitude

is scaled to the appropriate $\nabla T_e/\sqrt{\kappa_b} = 3.4$ using the same linear gradient dependence in figure 6(b) then the corresponding amplitude, marked by the 'X' symbol lies close to the extrapolated linear q dependence, which at least indicates consistency within the dataset.

5. Summary and discussion

Doppler reflectometry has been used to measure the frequency and amplitude of coherent oscillations in the $E \times B$ flow velocity in ASDEX Upgrade tokamak discharges. These oscillations are identified as GAMs from their frequency behaviour and are ubiquitously observed in ohmic and L-mode shots, but not in H-modes. The criteria for detecting the GAM is a sufficient level of turbulence (to both drive the GAM and to provide a measurable backscatter signal for the Doppler reflectometer diagnostic), and a not too high collisionality, i.e. $\omega_{GAM} > \nu_{ii}$.

Radially the GAM shows one or more amplitude maxima, coinciding with plateaus in the GAM frequency ω_{GAM} profile. These suggest a series of nested zonal rings, each a few cm wide; narrower in the edge and broader towards the core where profile gradients become shallower. If the GAM has a radial eigenmode structure then the spacing of adjacent plateaus maybe indicative of the mode half wavelength (cf. [29]). For the circular plasmas the radial wavelength would be $\lambda_r \sim \mathcal{O}(5-6)$ cm. The amplitude maxima ranges between $A_{GAM} = 0.2 - 0.8$ km s^{-1}, which can be several tens of percent of the mean perpendicular flow velocity. In terms of physical poloidal displacement, A_{GAM}/ω_{GAM}, this corresponds to peak-to-peak amplitudes of $0.4 - 1.0$ cm. The GAM is generally most intense in the edge density gradient region. Its outer extent is the plasma boundary or last-closed flux surface, its inner extent, however, is determined by the plasma configuration. For diverted high elongation plasmas with a flux-null or X-point the density profile has a well defined edge pedestal, i.e. a large second radial derivative in the profile, which appears to firmly restrict the inner radial reach of the GAM to the pedestal top. For non-diverted, i.e. limiter, configurations close to circular cross-section the density pedestal is weak and the profile approaches parabolic (i.e. small second radial derivatives) and multiple GAM maxima are observed deeper into the plasma. The inner radial extent is now dictated by the q profile. Raising the q profile allows a deeper reach - which is not inconsistent with a collisionless Landau-like damping dependence. In all cases, no GAMs are discernable where $q < 2$.

The actual dependence of the GAM amplitude on q, however, is more complex. For the low κ limiter configuration the GAM amplitude rises linearly with q. A roughly similar q dependence was also observed in numerical simulations by Angelino [18] using the ORB5 non-linear gyro-kinetic code. But, experimentally, for the high κ divertor shape the q relationship weakens, and may reverse slightly. This reduction in sensitivity to q with increasing elongation is also observed with the GAM frequency behaviour [10, 11]. Increasing the elongation also reduces the GAM amplitude - with an inverse dependence for the limiter configuration. Again, a similar reciprocal relationship with

κ is observed for the GAM frequency. In elongating the plasma the GAM maxima, (i.e. zonal region) moves radially inward to a lower q, however, the change in q is not sufficient to account for drop in A_{GAM} alone. There are several possible additional effects occurring here. The first candidate is the magnetic shear ($s = dq/dr$), which increases in the edge with κ_{b}. Enhanced magnetic shear damping of the turbulence was proposed by Kendl as the major cause of the reciprocal decrease in turbulent transport observed in gyro-fluid numerical simulations with increasing κ [30]. Also, while collisionless damping, $\gamma \propto \exp(-q^2)$, maybe dominant in the core, the effect of collisional damping (with a weaker q dependence: $\gamma \propto \nu_{ii}/q$) is certainly evident in the edge where the GAM disappears at high densities ($\nu^* \propto n/T^2$). There are other competing effects. Dissipation of the GAM energy into the parallel sound wave is always present but decreases towards the edge as $1/q$ [7]. The zonal flow (geodesic transfer) is not only a source of energy (drive) for the GAM but can also be a sink in coupling energy from the GAM back into the turbulence. In the edge, simulations indicate this to be a particularly important factor [7, 6]. Any, or all, of these factors may account for the experimental observations.

Nevertheless, a clear observation is that increasing the temperature/density gradient increases the GAM amplitude proportionately and reduces the global confinement, consistent with a raised turbulence level which both drives the GAM harder (via zonal flow/Reynolds stress coupling) and increases turbulent transport. But, from the data presented it is difficult to tell if the GAM is simply a signature of the turbulence (that is to say, the GAM features observed are those which are commensurate with maintaining the equilibrium of energy flow to the profile gradients and in turn to the turbulence and the GAM - and back), or if the GAM actually affects or reduces the turbulence. Certainly at the highest L-mode level the GAM amplitude is not insubstantial and, at the GAM frequencies observed, could play a role in enhancing the velocity shearing of the turbulence structures. Although numerical simulations have yet to demonstrate that the GAM activity is sufficient to affect the turbulence vorticity, i.e. shearing (cf. figure 15 in reference [6]), they do indicate that the GAM nevertheless acts as significant energy sink. However, whether the loss of the GAM in the H-mode is due simply to the much reduced turbulence level observed across the H-mode pedestal region, or is a consequence of other factors such as the higher mean $E_{\mathrm{r}} \times B$ velocity shearing also observed in the H-mode is still to be resolved. To address this problem of GAM/turbulence causality, and particularly the issue of self-suppression of edge turbulence by the GAM and, further, whether it has a role in triggering the transition to the enhanced confinement conditions in the H-mode, may be best approached via transient perturbative experiments.

Acknowledgments

We thank C.Tröster, J.Schirmer and W.Suttrop for assistance with the reflectometer hardware; B.Kurzan for Thomson scattering density, C.Maggi for CXRS ion

temperature, E.Wolfram for Li-beam density and M.Reich for Li-beam ion temperature profile validation; plus B.Scott and K.Hallatschek for fruitful discussions.

References

[1] Diamond P H, Itoh S-I, Itoh K and Hahm T S 2005 *Plasma Phys. Control. Fusion* **47** R35
[2] Conway G D, Scott B, Schirmer J, Reich M, Kendl A and ASDEX Upgrade Team 2005 *Plasma Phys. Control. Fusion* **47** 1165
[3] Scott B 2003 *Phys. Lett. A* **320** 53
[4] Hahm T S, Beer M A, Lin Z, Hammett G W, Lee W W and Tang W M 1999 *Phys. Plasmas* **6** 922
[5] Hahm T S, Burrell K H, Lin Z, Nazikian R and Synakowski E J 2000 *Plasma Phys. Control. Fusion* **42** A205
[6] Scott B D 2005 *New J. Phys.* **7** 92
[7] Miyato N, Kishimoto Y and Li J 2004 *Phys. Plasmas* **11** 5557
[8] Winsor N, Johnson J L and Dawson J M 1968 *Phys. Fluids* **11** 2448
[9] McKee G R, Gupta D K, Fonck R J, Schlossberg D J, Shafer M W, and Gohil P 2006 *Plasma Phys. Control. Fusion* **48** S123
[10] Conway G D, Tröster C, Scott B, Hallatschek K and ASDEX Upgrade Team 2007 *Proc. 34th EPS Conf. Plasma Phys. (Warsaw)* ECA vol 31F (Mulhouse: EPS) O-4.009
[11] Conway G D, Tröster C, Scott B, Hallatschek K and ASDEX Upgrade Team 2008 *Plasma Phys. Control. Fusion* **50** 055009
[12] Conway G D *et al* 2006 *Proc. 21st IAEA Fusion Energy Conf. (Chengdu)* (Vienna: IAEA) IAEA-CN-149/EX/2-1, http://www-pub.iaea.org/MTCD/Meetings/FEC2006/ex_2-1.pdf
[13] Ido T *et al* 2006 *Plasma Phys. Control. Fusion* **48** S41
[14] Yan L W *et al* 2007 *Nucl. Fusion* **47** 1673
[15] Lebedev V B, Yushmanov P N, Diamond P H, Novakovskii S V and Smolyakov A I 1996 *Phys. Plasmas* **3** 3023
[16] Watari T, Hamada Y, Fujisawa A, Toi K and Itoh K 2005 *Phys. Plasmas* **12** 062304
[17] Itoh K, Hallatschek K and Itoh S-I 2005 *Plasma Phys. Control. Fusion* **47** 451
[18] Angelino P, Bottino A, Hatzky R, Jolliet S, Sauter O, Tran T M and Villard L 2006 *Plasma Phys. Control. Fusion* **48** 557
[19] Novakovskii S V, Liu C S, Sagdeev R Z and Rosenbluth M N 1997 *Phys. Plasmas* **4** 4272
[20] Kim E-J and Diamond P H 2004 *Phys. Plasmas* **11** L77
[21] Hallatschek K 2006 *Proc. 21st IAEA Fusion Energy Conf. (Chengdu)* (Vienna: IAEA) IAEA-CN-149/TH/2-6, http://www-pub.iaea.org/MTCD/Meetings/FEC2006/th_2-6.pdf
[22] Conway G D, Schirmer J, Klenge S, Suttrop W, Holzhauer E and ASDEX Upgrade Team 2004 *Plasma Phys. Control. Fusion* **46** 951
[23] Conway G D, Angioni C, Dux R *et al* 2006 *Nucl. Fusion* **46** S799
[24] Conway G D *et al* 2007 *Proc. 8th Intl. Reflectometry Wksh. for fusion plasma diagnostics IRW8 (St.Petersburg)* p30, http://www.aug.ipp.mpg.de/IRW/IRW8
[25] McCarthy P J 1999 *Phys. Plasmas* **6** 3554
[26] Liewer P C 1985 *Nucl. Fusion* **25** 543
[27] Neuhauser J *et al* 2002 *Plasma Phys. Control. Fusion* **44** 855
[28] Mertens V, Raupp G and Treutterer W 2003 *Fusion Sci. Tech.* **44** 593
[29] Krämer-Flecken A, Soldatov S, Zimmermann O and TEXTOR-Team 2007 *Proc. 8th Intl. Reflectometer Wksh. for fusion plasma diagnostics IRW8 (St.Petersburg)* p89, http://www.aug.ipp.mpg.de/IRW/IRW8
[30] Kendl A and Scott B D 2006 *Phys. Plasmas* **13** 012504